

GLPU: A GEOMETRIC APPROACH FOR LIDAR POINTCLOUD UPSAMPLING

George Eskandar[†], Janaranjani Palaniswamy[†], Karim Guirguis^{*}, Barath Somashekar[†], Bin Yang[†]

[†]University of Stuttgart, Institute of Signal Processing and System Theory, Stuttgart, Germany

^{*} Robert Bosch GmbH, Renningen, Germany

ABSTRACT

In autonomous driving, lidar is inherent for the understanding of the 3D environment. Lidar sensors vary in vertical resolutions, where a denser pointcloud depicts a more detailed environment, albeit at a significantly higher cost. Pointcloud upsampling predicts high-resolution pointclouds from sparser ones to bridge this performance gap at a lower cost. Although many upsampling frameworks have achieved a robust performance, a fair comparison is difficult as they were tested on different datasets and metrics. In this work, we first conduct a consistent comparative study to benchmark the existing algorithms on the KITTI dataset. Then, we observe that there are three common factors that hinder the performance: an inefficient data representation, a small receptive field, and low-frequency losses. By leveraging the scene geometry, a new self-supervised geometric lidar pointcloud upsampling (GLPU) framework is proposed to address the aforementioned limitations. Our experiments demonstrate the effectiveness and superior performance of GLPU compared to other techniques on the KITTI benchmark.

Index Terms— pointcloud upsampling, GANs, lidar

1. INTRODUCTION

Light detection and ranging (LiDAR) pointclouds are vital for 3D perception and geometrical understanding of a surrounding environment for autonomous vehicles. Numerous tasks are dependent on 3D information from lidar, such as 3D object detection [1–5], 3D semantic segmentation [6], localization [7], mapping [8] and path planning [9]. Mounted on the vehicle, lidar rotates around a vertical axis and emits pulses of infrared light waves to retrieve accurate 3D measurements. Although the horizontal resolution of lidar is high, the vertical resolution is usually low and depends on the number of channels present in the sensor (16, 32, 64 and 128 typically). Denser pointclouds in the vertical direction provide more cues about the geometry of the environment, albeit the sensors come at a significantly higher cost [10]. Upsampling lidar in the vertical resolution can help alleviate this issue and optimize the trade-off between cost and performance.

To this end, we focus on lidar super-resolution as a generative task that can help improve downstream perception tasks

like 3D object detection, point segmentation, and/or domain adaptation [11–13]. Recently, there has been a growing interest in developing generative models for lidar based on VAEs and GANs [14]. A similar line of work, namely sequential lidar prediction [15–18], aims to improve the trajectory forecasting task by generating future lidar pointclouds.

Although many pointcloud super-resolution algorithms have achieved remarkable performance, there are 3 main challenges that prevent us from assessing which methods work better for lidar in autonomous driving. First, many pointcloud algorithms [19–22] were tested on datasets containing synthetic objects with fewer points ($\sim 10k$) than a typical lidar scan ($\sim 100k$). Second, different evaluation metrics were used for various models. Third, the downsampling and upsampling schemes of these algorithms were different. For example, methods based on Pointnet operators [19–23] sample patches from the pointclouds with farthest sampling, downsample each patch and train their corresponding networks on upsampling the low-resolution patches. In contrast, [14] removes points from lidar scan with a uniform probability distribution and the whole pointcloud is reconstructed directly with a VAE [24]. A third scheme is presented in [10, 25], whereby lidar scans are downsampled in the vertical resolution by skipping every second beam and a 2D convolutional network attempts to upsample the pointcloud. In this work, we present a unified testbed for assessing the different pointcloud upsampling algorithms. We classify the methodologies into 2 groups: point-based and grid-based methods. The former use PointNet operations directly on the pointcloud, while the latter project the pointcloud on image coordinates and deploy 2D convolutional networks. Our empirical evaluations show that attempting to learn an upsampled pointcloud in an end-to-end manner with deep learning while neglecting the scene geometry hinders the performance. To circumvent these limitations, we propose the Geometric Lidar Pointcloud Upsampling (GLPU) framework that attends to the scene 3D geometry to enhance the results. Namely, we consider and improve 3 factors: the geometric representation of the pointcloud before the network, the receptive field of the network’s backbone and the loss function learned by the network. Comparative qualitative and quantitative analyses are conducted to illustrate the performance of our model on KITTI [26] dataset.

2. OVERVIEW OF UPSAMPLING ALGORITHMS

In this section, we first outline the employed training and evaluation pipelines, followed by an analysis of the results. Formally, let \mathcal{P} be the input pointcloud with \mathcal{N} points, where $\mathcal{P} = \{(x, y, z)_i : i = 1, \dots, \mathcal{N}\}$, and z is the vertical height. We can project \mathcal{P} onto 2D image coordinates (u, v) resulting in a range image representation, \mathcal{Q} . We define (H, W) to be the height and width of \mathcal{Q} , $f = f_{up} + f_{down}$ the vertical field-of-view of the lidar sensor, $r = \sqrt{x^2 + y^2 + z^2}$ the range of the point and $d = \sqrt{x^2 + y^2}$ the radial distance. The projection can be expressed in Eq. (1) as follows:

$$\begin{aligned} u &= \frac{1}{2}[1 - \arctan(y, x)\pi^{-1}]W, \\ v &= [1 - (\arcsin(zr^{-1}) + f_{up})f^{-1}]H. \end{aligned} \quad (1)$$

The range image representation is suitable for the vertical downsampling of the image since each row in \mathcal{Q} represents a lidar beam. Moreover, it is an invertible transformation. A range image \mathcal{Q} is commonly represented in spherical coordinates $(\mathcal{Q}_{u,v} = r)$ [4, 6, 10, 25, 27]; however, polar $(\mathcal{Q}_{u,v} = (d, z))$ and cartesian $(\mathcal{Q}_{u,v} = (x, y, z))$ coordinates can also be used as in [14].

We train all models on a $\times 4$ -upsampling factor in a self-supervised way: every 4th row in \mathcal{Q} is sampled, and the resulting low-resolution range image \mathcal{Q}_{LR} is fed to each model. For point-based algorithms, \mathcal{Q}_{LR} is transformed back to a pointcloud \mathcal{P}_{LR} ; otherwise, it is directly used by grid-based methods. All models are trained with their original hyperparameters using their officially published codes. We choose the Raw KITTI dataset [26] as the benchmark. The lidar sensor in KITTI is the Velodyne HDL64, which has a 64-lines resolution and around 1600 points approximately per line. However, processing this resolution with point-based methods is computationally hefty. To ensure a fair comparison between all algorithms, we limit the size of the pointcloud to 10k points (40×256) using the preprocessing of [14]. We use the train/validation/test ($40k/80/700$) split used by [14, 28]. While grid-based methods for lidar upsampling [10, 25] have used 2D-metrics like mean absolute error (MAE) or root mean square error (RMSE) on the range image to evaluate the performance, point-based methods have mainly used the earth-moving distance (EMD) and chamfer distance (CD) [29], because they measure distance between subsets in \mathcal{R}^3 . Moreover, it has been shown in [30] that EMD strongly correlates with perceptual quality, all of which motivates the use of EMD and CD for consistent model evaluation. We present the results in Tab. 1.

From Tab. 1, we can observe that point-based methods underperform on lidar upsampling, especially when trained from scratch on lidar. All models, except PUNet, do not converge during training. For further investigation, we evaluate point-based models pre-trained on the PUNet dataset [19]. Surprisingly, the pretrained PUGAN, 3PU and ARGCN per-

Table 1: Quantitative comparisons on Kitti Benchmark, $\times 4$ upsampling rate

	Framework	Pretrained ¹	EMD	CD
Point-based	3PU [21]	✓	1265	6.58
	3PU [21]	✗	924	6.37
	PUGAN [20]	✗	866	77.82
	ARGCN[22]	✗	829	29.07
	PUGAN [20]	✓	385	0.86
	PUNet [19]	✓	371	1.70
	ARGCN [22]	✓	265	0.73
Grid-based	PUNet [19]	✗	241.6	0.67
	cVAE [14]	✗	272.3	1.12
	SRResNet [25]	✗	100.1	0.052
	Unet [10]	✗	101.0	0.054

¹ Pretrained on PU-Net dataset

form better although no lidar scan was seen during pretraining. By looking at the upsampled pointclouds in Fig. 2, we can see that, except for PUNet, no point-based method was able to replicate the lidar scan pattern. The upsampled pointclouds exhibit higher density around each line, but no new lines are added in between. We hypothesize that these networks are not able to reproduce the scan pattern by architectural design, and hence do not converge during training.

In order to understand why PUNet is the only point-based method that could replicate the scan pattern, we inspect and compare the architectures of point-based models. In general, each network can be modeled as being composed of 3 parts: (i) a feature extraction backbone, (ii) a feature expansion module, and (iii) pointset generation layer. Although these parts are different across all models, it is the feature extractor of PUNet that is distinct from other algorithms due to its hierarchical design. In PUNet, point features are computed at different scales, followed by a multi-level feature aggregation resulting in a wide receptive field that captures both local and global information in the pointcloud. Subsequent architectures like PUGAN, 3PU and ARGCN have small receptive fields, an intentional design choice that outperforms PU-Net on single object datasets which feature uniformly distributed pointclouds in the 3D space. However, lidar pointclouds are not uniform by design, and a local receptive field that does not span across different vertical lines will lead to the generation of points closer to the input points which does not mimic a lidar scan pattern.

On the other hand, grid-based methods benefit from the range image representation, which intrinsically models the lidar scan pattern. Their good performance can be attributed to the fact that even small receptive fields span different lidar beams vertically. In addition, they are more computationally efficient making them suitable for real-time constraints. However, they suffer from the smoothing effects from convolutional layers, blurring edges and object boundaries. Moreover, the standard use of MAE and MSE losses in these methods [10, 25] does not encourage the upsampling layer to produce high-frequencies in the range image, potentially leading

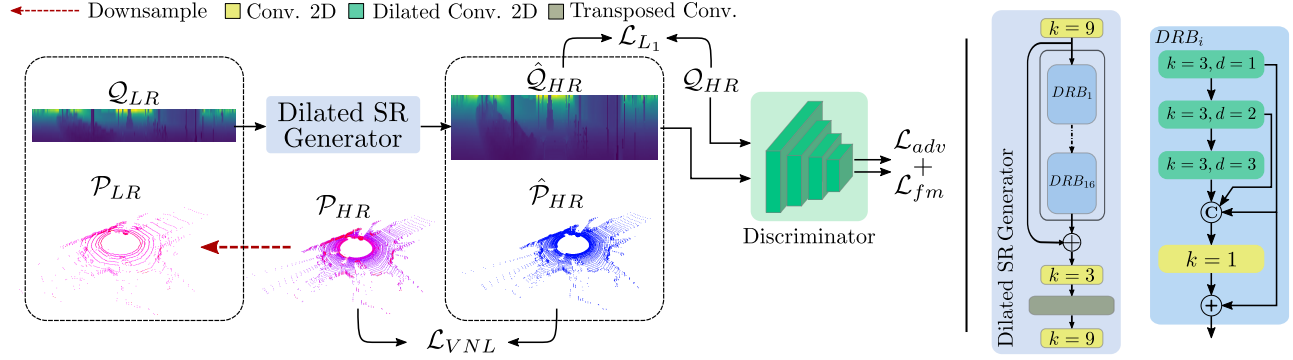


Fig. 1: Proposed Methodology. *Left*, the whole architecture and losses are presented. *Right*, the generator and DRB are depicted.

to the loss of fine details in the scene that are relevant to identify sparser classes (pedestrians and cyclists). These effects were mitigated to an extent either by leveraging pretrained point segmentation networks in [25], or in [10] by employing a Bayesian deep network to decrease overfitting. Arguably, it is desirable to develop an upsampling algorithm that leverages geometry instead of semantics not to incur the costs of extra-labels, while enabling faster inference (unlike bayesian inference in [10], which is more computationally expensive).

3. PROPOSED METHODOLOGY

Motivated by the previous findings, we propose a model GLPU that addresses the previous limitations and harvests the advantages of both point-based and grid-based methods through a careful consideration of the 3D scene geometry.

3.1. Range image representation with polar coordinates

As previously noted, the choice of the pointcloud representation is crucial for the upsampling performance. The range image representation is a better fit for the task: first, 2D networks are not as computationally expensive as pointnet operations and second, it allows conv layers with small receptive fields to interpolate between vertical lines. However, the latter comes with a disadvantage: the distribution of distances exhibits a large variance in the vertical direction H of the range image (the issue was also mentioned by [31]), impeding conv and upsampling layers from replicating these high-frequency components in the range image. The problem is further complicated by the use of spherical coordinates, whereby it's implicitly assumed that the elevation angle $\theta = \arcsin(zr^{-1})$ is constant between all vertical lines. This assumption is not true and it introduces a quantization error when the inverse transformation from Q to \mathcal{P} is applied, namely $z = r\sin(\theta)$. We argue that it is more beneficial for the network to directly observe and learn the polar or cartesian coordinates, similar to the point-based operations, in order to eliminate this quantization error from the upsampling error. We thus choose to represent the lidar scene as range image with polar coordinates. This representation is used for the input and output of the network.

3.2. Dilated SR-ResNet

The second most important factor we have observed is the receptive field, which should capture local and global information in the pointcloud. The receptive field of the SRResNet in [25] is large enough in H but not in W . On the other hand, the receptive field of the UNet in [10] is large enough by virtue of the average pooling operations used but does not offer an advantage over SRResNet. Classes like pedestrians and cyclists which are very small compared to the whole lidar scene, might disappear after the average pooling. It is thus desirable to have a large receptive field without increasing the stride. Since naively increasing the kernel size will greatly increase the number of parameters in the network, we build our SRResNet-based generator architecture using the dilated residual blocks introduced in [4] as can be seen in Fig. 1. The dilated convolutions increase the size of the receptive field to detect objects of different scales without significantly increasing the number of parameters. The parallel design of the block also allows to flexibly capture coarse and fine details.

3.3. High-frequency Losses

In order to foster the generation of high-frequency components in the range image, we train the network adversarially, inspired by the SRGAN [32] framework for images. However, using the same discriminator architecture and GAN loss leads to unstable training. We remove the last average pooling and conv layers, so the discriminator becomes a patch discriminator and replace the l_2 GAN loss by the one in [33] and a feature-matching loss [34]. Empirically, we find that this GAN setup is more stable for lidar scans. In order to force the upsampling layer (transposed conv layer) to produce more meaningful features, we penalize the deviation of the surface normal of the generated pointcloud from that of the groundtruth. However, instead of calculating the normal vector for every point in the range image, we use the virtual normal loss (VNL) proposed by [35]. Specifically, k groups of 3 non-collinear points are sampled from the pointcloud and the normal vector to the plane formed by triplet is computed. The final loss comprises both 3D losses (VNL) and 2D losses (L_1 -loss with respect to the groundtruth range map and ad-

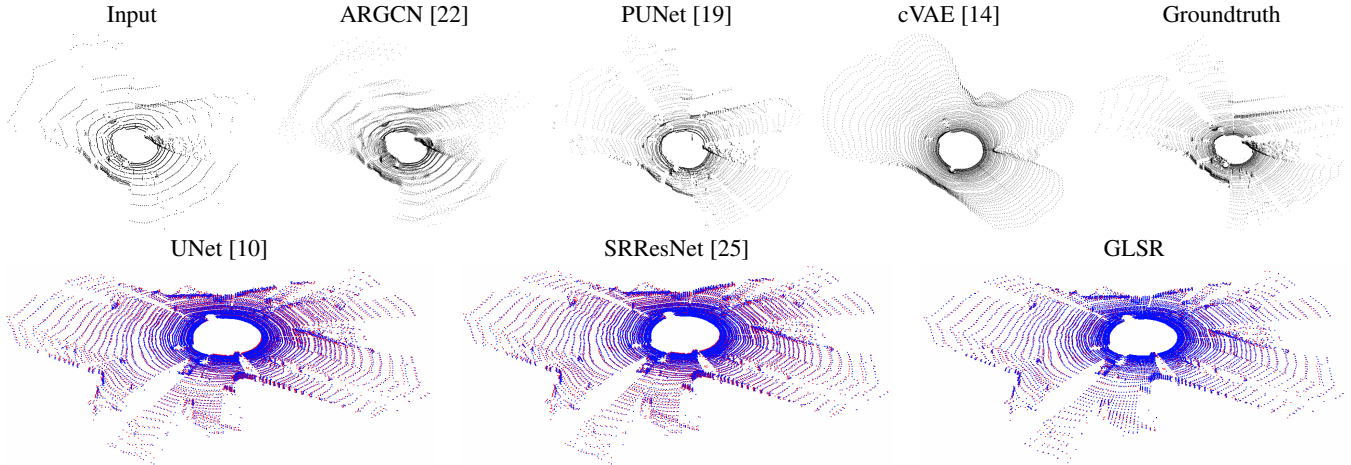


Fig. 2: Qualitative Results. *Upper Row.* Generated lidar scans from point and grid-based models. *Lower Row.* Comparison of the three best performing models. Generated pointclouds are depicted in blue and the groundtruth is overlaid in red. Thus, the bluer the pointcloud is, the higher its quality.

versarial losses).

4. RESULTS

We train on our model for 100 epochs, with a batchsize of 32 and ADAM optimizer with learning rate of 0.0001. We perform and ablation study and report the results in Tab. 2 and Fig. 2. We also add the metrics MAE and RMSE to Tab. 2. MAE and RMSE are measured in meters, while CD is measured in m^2 . Lower values indicate superior performance.

The results show that the proposed model outperforms the state-of-the-art on the EMD, CD and MAE metrics and is on par on the RMSE metrics. However, we find that MAE and RMSE are not sufficient to judge the upsampling quality: the table shows that EMD and CD can differ significantly, while MAE and RMSE exhibit little variations. This observation is analogous to the findings in [32] for RGB images. We notice that the UNet model [10] underperforms the basic SRResNet [25] on the proposed benchmark, contrary to the findings in [10]. We attribute this difference to the fact that synthetic lidar obtained from the CARLA simulator [36] was used for evaluation in [10], which is less noisier than real lidar data.

In Tab. 2, an ablation study on our model showcases the contribution of each design choice. Although, the SRGAN itself does not improve the results significantly, when combined with the VNL, a clear reduction in EMD and CD can be seen. The proposed losses guide the generator to produce a more coherent scene by enforcing a high-order constraint on the underlying scene geometry. The use of polar coordinates is shown to further improve the results, since it removes the vertical quantization error. On the other hand, cartesian coordinates do not show an improvement arguably because regressing 3 channels is a more challenging task for the network. Finally, we find that the DRBs further enhance the performance, confirming our claim that the receptive field is a crucial design parameter for the task.

Table 2: Comparative and Ablation study on Kitti Benchmark, x4 upsampling rate. The last row represents the complete proposed framework

Framework	EMD	CD	MAE	RMSE
SRResNet [25]	100.1	0.052	0.20	0.86
UNet [10]	101.0	0.054	0.21	0.85
SRGAN [32]	100.6	0.051	0.19	0.86
+ VNL	88.7	0.031	0.23	0.87
+ VNL + cartesian	89.6	0.033	0.24	0.88
+ VNL + polar	84.3	0.023	0.21	0.86
+ DRB + VNL + polar (GLPU)	81.4	0.016	0.18	0.87

5. CONCLUSION

In this work, a study of different lidar upsampling algorithms was conducted. Our findings revealed that point-based algorithms cannot reproduce the lidar scan pattern, unless they have a global receptive field. However, we suggest they can be used to produce denser pointclouds for foreground objects if they can become less memory-intensive. We proposed a grid-based method that leverages: geometric losses, polar coordinates for better pointclouds representation, and an architecture that enables a flexible and extended receptive field. Strong performance was demonstrated on the proposed benchmark. However, this work is not without limitations. The proposed method needs to be tested on lidar scenes with a non-uniform vertical downsampling scheme. We plan to extend our method to work on pointclouds with a bigger horizontal resolution and to validate the method in a domain adaptation setting. .

Acknowledgement

The research leading to these results is funded by the German Federal Ministry for Economic Affairs and Energy within the project "AI Delta Learning". The authors would like to thank the consortium for the successful cooperation.

References

- [1] Shaoshuai Shi et al. “PV-RCNN: Point-Voxel Feature Set Abstraction for 3D Object Detection”. In: *Proceedings of the IEEE Conference on Computer Vision and Pattern Recognition*. 2020.
- [2] Alex H. Lang et al. “PointPillars: Fast Encoders for Object Detection from Point Clouds”. In: *CVPR*. 2019.
- [3] Yan Yan, Yuxing Mao, and Bo Li. “SECOND: Sparsely Embedded Convolutional Detection”. In: *Sensors (Basel, Switzerland)* 18 (2018).
- [4] Zhidong Liang et al. “RangeRCNN: Towards Fast and Accurate 3D Object Detection with Range Image Representation”. In: *ArXiv abs/2009.00206* (2020).
- [5] Wu Zheng et al. “SE-SSD: Self-Ensembling Single-Stage Object Detector From Point Cloud”. In: *2021 IEEE/CVF Conference on Computer Vision and Pattern Recognition (CVPR)* (2021), pp. 14489–14498.
- [6] Andres Milioto et al. “RangeNet ++: Fast and Accurate LiDAR Semantic Segmentation”. In: *2019 IEEE/RSJ International Conference on Intelligent Robots and Systems (IROS)* (2019), pp. 4213–4220.
- [7] Xieyuanli Chen et al. “Range Image-based LiDAR Localization for Autonomous Vehicles”. In: *2021 IEEE International Conference on Robotics and Automation (ICRA)* (2021), pp. 5802–5808.
- [8] Ignacio Vizzo et al. “Poisson Surface Reconstruction for LiDAR Odometry and Mapping”. In: *2021 IEEE International Conference on Robotics and Automation (ICRA)* (2021), pp. 5624–5630.
- [9] Wenjie Luo, Binh Yang, and Raquel Urtasun. “Fast and Furious: Real Time End-to-End 3D Detection, Tracking and Motion Forecasting with a Single Convolutional Net”. In: *2018 IEEE/CVF Conference on Computer Vision and Pattern Recognition* (2018), pp. 3569–3577.
- [10] Tixiao Shan et al. “Simulation-based lidar super-resolution for ground vehicles”. In: *Robotics and Autonomous Systems* 134 (Dec. 2020), p. 103647. DOI: 10.1016/j.robot.2020.103647.
- [11] Yan Wang et al. “Train in Germany, Test in the USA: Making 3D Object Detectors Generalize”. In: *2020 IEEE/CVF Conference on Computer Vision and Pattern Recognition (CVPR)* (2020), pp. 11710–11720.
- [12] Jihan Yang et al. “ST3D: Self-training for Unsupervised Domain Adaptation on 3D Object Detection”. In: *Proceedings of the IEEE/CVF Conference on Computer Vision and Pattern Recognition*. 2021.
- [13] Xingyi Zhou et al. “Unsupervised Domain Adaptation for 3D Keypoint Estimation via View Consistency”. In: *ECCV*. 2018.
- [14] Lucas Caccia et al. “Deep Generative Modeling of LiDAR Data”. In: *2019 IEEE/RSJ International Conference on Intelligent Robots and Systems (IROS)* (2019), pp. 5034–5040.
- [15] Xinshuo Weng et al. “Inverting the Forecasting Pipeline with SPF2: Sequential Pointcloud Forecasting for Sequential Pose Forecasting”. In: *Proceedings of (CoRL) Conference on Robot Learning*. 2020.
- [16] Fan Lu et al. “MoNet: Motion-Based Point Cloud Prediction Network”. In: *IEEE Transactions on Intelligent Transportation Systems PP* (Dec. 2021), pp. 1–11. DOI: 10.1109/TITS.2021.3128424.
- [17] B. Mersch et al. “Self-supervised Point Cloud Prediction Using 3D Spatio-temporal Convolutional Networks”. In: *Proceedings of (CoRL) Conference on Robot Learning (CoRL)*. 2021.
- [18] George Eskandar et al. “SLPC: A VRNN-based approach for stochastic lidar prediction and completion in autonomous driving”. In: *2021 29th European Signal Processing Conference (EUSIPCO)* (2021), pp. 721–725.
- [19] Lequan Yu et al. “PU-Net: Point Cloud Upsampling Network”. In: *2018 IEEE/CVF Conference on Computer Vision and Pattern Recognition* (2018), pp. 2790–2799.
- [20] Ruihui Li et al. “PU-GAN: A Point Cloud Upsampling Adversarial Network”. In: *2019 IEEE/CVF International Conference on Computer Vision (ICCV)* (2019), pp. 7202–7211.
- [21] Wang Yifan et al. “Patch-Based Progressive 3D Point Set Upsampling”. In: *2019 IEEE/CVF Conference on Computer Vision and Pattern Recognition (CVPR)*. 2019, pp. 5951–5960.
- [22] Huikai Wu and Kaiqi Huang. “Point Cloud Super Resolution with Adversarial Residual Graph Networks”. In: *31st British Machine Vision Conference 2020, BMVC*. BMVA Press, 2020.
- [23] C. Qi et al. “PointNet: Deep Learning on Point Sets for 3D Classification and Segmentation”. In: *2017 IEEE Conference on Computer Vision and Pattern Recognition (CVPR)* (2017), pp. 77–85.
- [24] Diederik P. Kingma and Max Welling. “Auto-Encoding Variational Bayes”. In: *2nd International Conference on Learning Representations, ICLR 2014*. 2014.
- [25] Larissa T. Triess et al. “CNN-based synthesis of realistic high-resolution LiDAR data”. In: *2019 IEEE Intelligent Vehicles Symposium (IV)*. 2019, pp. 1512–1519.
- [26] Andreas Geiger, Philip Lenz, and Raquel Urtasun. “Are we ready for Autonomous Driving? The KITTI Vision Benchmark Suite”. In: *Conference on Computer Vision and Pattern Recognition (CVPR)*. 2012.
- [27] Larissa T. Triess et al. “Scan-based Semantic Segmentation of LiDAR Point Clouds: An Experimental Study”. In: *2020 IEEE Intelligent Vehicles Symposium (IV)* (2020), pp. 1116–1121.
- [28] William Lotter, Gabriel Kreiman, and David Cox. “Deep Predictive Coding Networks for Video Prediction and Unsupervised Learning”. In: *ICLR*. 2017.
- [29] Haoqiang Fan, Hao Su, and Leonidas J. Guibas. “A Point Set Generation Network for 3D Object Reconstruction from a Single Image”. In: *2017 IEEE Conference on Computer Vision and Pattern Recognition (CVPR)* (2017), pp. 2463–2471.
- [30] Panos Achlioptas et al. “Learning Representations and Generative Models for 3D Point Clouds”. In: *ICML*. 2018.
- [31] Larissa Triess, David Peter, and Johann Marius Zöllner. “Semi-Local Convolutions for LiDAR Scan Processing”. In: *I (Still) Can’t Believe It’s Not Better! NeurIPS 2021 Workshop*. 2021. URL: <https://openreview.net/forum?id=rSGfLc2w4Z>.
- [32] Christian Ledig et al. “Photo-Realistic Single Image Super-Resolution Using a Generative Adversarial Network”. In: *2017 IEEE Conference on Computer Vision and Pattern Recognition (CVPR)*. 2017, pp. 105–114.
- [33] Tero Karras et al. “Analyzing and Improving the Image Quality of StyleGAN”. In: *2020 IEEE/CVF Conference on Computer Vision and Pattern Recognition (CVPR)* (2020), pp. 8107–8116.
- [34] Ting-Chun Wang et al. “High-resolution image synthesis and semantic manipulation with conditional GANs”. In: *Conference on Computer Vision and Pattern Recognition (CVPR)*. 2018.
- [35] Wei Yin, Yifan Liu, and Chunhua Shen. “Virtual Normal: Enforcing Geometric Constraints for Accurate and Robust Depth Prediction”. In: *IEEE transactions on pattern analysis and machine intelligence PP* (2021).
- [36] Alexey Dosovitskiy et al. “CARLA: An Open Urban Driving Simulator”. In: *Proceedings of the 1st Annual Conference on Robot Learning*. 2017, pp. 1–16.